sustainability

MDPI

Article

Optimizing Integrated Water and Electrical Networks through a Holistic Water–Energy Nexus Approach

Mennatalla Elbalki [1], Mostafa F. Shaaban [1], Ahmed Osman [1], Ariana Pietrasanta [2], Mohammed Kamil [3] and Abdelfatah Ali [1,4,*]

[1] Department of Electrical Engineering, American University of Sharjah, Sharjah 26666, United Arab Emirates; g00093037@alumni.aus.edu (M.E.); mshaaban@aus.edu (M.F.S.); aosmanahmed@aus.edu (A.O.)
[2] INGAR Instituto de Desarrollo y Diseño (CONICET-UTN), Santa Fe 3000, Argentina; apietrasanta@aus.edu
[3] Department of Mechanical and Nuclear Engineering, University of Sharjah, Sharjah 27272, United Arab Emirates; mmohammed@sharjah.ac.ae
[4] Department of Electrical Engineering, South Valley University, Qena 83523, Egypt
* Correspondence: abdelfatahm@aus.edu

Abstract: As water and electrical networks cannot be entirely independent, a more integrated approach, the water–energy nexus (WEN), is developed. A WEN is the basis of a smart city where water and electrical networks are interconnected and integrated by implementing efficient management strategies. Accordingly, this study develops a dynamic co-optimization model for designing and operating an integrated power and water system. The proposed co-optimization model minimizes the total annual and operational costs of a micro-WEN system while capturing its optimum design values and operating conditions and meeting the demands of the electrical and water networks. Furthermore, this work presents a plan for transitioning from thermal desalination to reverse osmosis (RO) desalination in the United Arab Emirates (UAE). The key objective is to decouple electricity and water production, effectively tackling the issue of operating the UAE's power plants at low efficiency during the winter while ensuring an adequate water supply to meet the growing demand. The results show that the co-optimization model provides a significant reduction in the total operational cost with the integration of photovoltaic energy and shifting to RO. Most importantly, the micro-WEN system is optimized over multiple timescales to reduce the computation effort and memory requirements.

Keywords: non-linear programming; optimization; multi-effect distillation; combined-cycle power plants; reverse osmosis; water–energy nexus

Citation: Elbalki, M.; Shaaban, M.F.; Osman, A.; Pietrasanta, A.; Kamil, M.; Ali, A. Optimizing Integrated Water and Electrical Networks through a Holistic Water–Energy Nexus Approach. *Sustainability* **2024**, *16*, 3783. https://doi.org/10.3390/su16093783

Academic Editor: Andrea G. Capodaglio

Received: 12 March 2024
Revised: 14 April 2024
Accepted: 20 April 2024
Published: 30 April 2024

1. Introduction

The term water–energy nexus (WEN) describes the interdependence of water and energy systems. Considering a smaller scale, the micro water–energy nexus integrates the electrical network and the water network to act as a single entity in a microgrid. This interdependence has become increasingly important as the world faces challenges such as population growth, urbanization, and climate change, which pressure water and energy systems. As the world's population is projected to increase by 2 billion people by 2050, leading to an increased demand for water and electricity, approximately 40% of the world's population is anticipated to suffer from the issue of water scarcity [1]. Consequently, water and power operations and systems must be planned simultaneously, considering the water–energy nexus in decision-making and developing integrated water and energy management strategies to address these challenges. This entails investigating ways to optimize the use of water in energy production, enhancing the energy efficiency of water infrastructure, and creating integrated water and energy management techniques that can help ensure a sustainable and resilient water–energy system [1–4].

The integration of thermal desalination of seawater in combined-cycle power generation plants (CCPPs) has been indicated as a promised enhancement in power generation

and water desalination. However, in order to minimize the operational cost of the WEN system and optimize the utilization of energy resources fed to the power plant, advanced resource management must be developed.

The UAE has limited natural water resources and uses desalination as the dominant technology to make seawater potable. Thermal desalination and reverse osmosis (RO) are the two leading desalination technologies [5–7]. Thermal desalination has two primary types, namely, multi-effect distillation (MED) and multi-stage flash (MSF) distillation, which are conventionally a part of a combined-cycle or a cogeneration power plant [8]. Cogeneration is a system that utilizes one primary energy source to produce two or more useful forms of energy at once. For example, in a combined-cycle gas turbine (CCGT), a gas turbine converts mechanical energy into electricity and exhausts waste heat, which a steam turbine uses to generate additional electricity [9–12]. The steam turbine produces electric energy and supplies a tremendous amount of low-pressure steam [13]. As thermal energy is an essential energy input to produce freshwater, the MED and MSF desalination processes and electricity generation are integrated on the same site with the aim of satisfying demand from water and electric energy, respectively.

Thus, the thermal desalination of seawater supplies the majority of residential and industrial water needs in the UAE. Consequently, electricity generation is associated with water production from the combined-cycle cogeneration thermal plants. Currently, during winter, when the electric demand is severely reduced, the UAE has to operate its power plants at low efficiency to be able to meet the water demand that stays almost the same throughout the year, as shown in Figure 1. The major target currently is to decouple electricity and water production by phasing out the cogeneration plants and shifting from thermal desalination to RO.

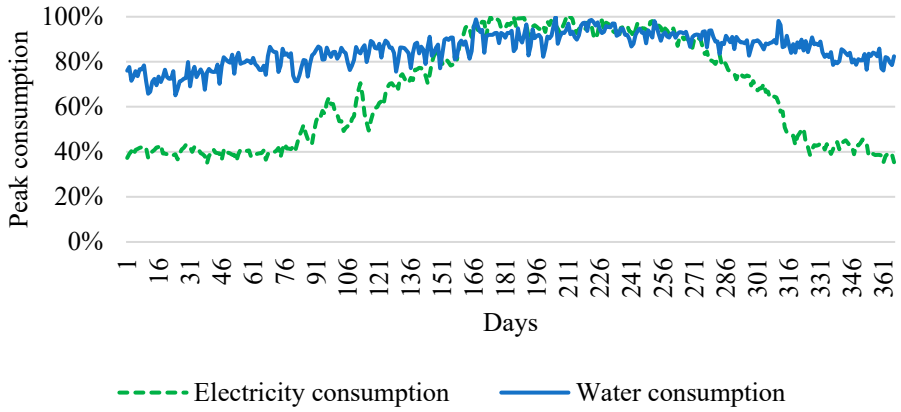

Figure 1. UAE's electricity and water consumption per day in a year.

Several water–energy nexus concepts have been investigated in the literature to model the integration and co-optimization of electrical and water networks. The authors of [14] use Bender's decomposition method to model a robust two-stage operation that manages the water–energy nexus system at the distribution level to reduce the operational cost. However, the work assumes that the electrical, gas, and water networks are owned by a single entity. An optimization model is designed for integrated water and electricity systems for a remote island that does not have access to the utility networks to fulfill the electricity and water demands with three different desalination technologies, including MED, MSF, and RO [15].

In [16], a new optimization model is proposed to minimize the operational costs of an integrated water–energy nexus system where wind turbines generate power and RO desalinates water. This work simplifies the mixed-integer non-linear programming (MNLP) model and utilizes General Algebraic Mathematical Software (GAMS 42) to attain results with greater accuracy. Considering the uncertainty arising from wind generation outputs, the work in [17] proposes a robust operation model for a multi-energy WEN in which the

energy system involves natural gas transmission, district heating, a power transmission network, and a water distribution network (WDN).

Also, in [18], Moazeni and Khazaei develop a co-optimization MNLP model by combining the wastewater treatment plant's demand response and the residential loads in the smart grid's economic dispatch. The proposed model minimizes the amount of energy consumed by the wastewater treatment plant and the cost of the generated power of the smart grid, resulting in high-quality treated wastewater. In [19], the authors introduce the integration of water desalination within security-constrained unit commitment (SCUC), which significantly minimizes the system's operational cost, especially with the enormous desalination size. As the water–energy nexus concept is mainly applied at the supply side, in [20], the work considers the interconnections between water and energy demands in a reservoir to propose new supply-side management of optimal and smart hydro reservoirs and uses advanced neural networks to predict two different scenarios that simulate the annual operation and remote monitoring situations.

Several WEN approaches are investigated on the demand side. For instance, Fooladivanda et al. [21] emphasize the importance of pump scheduling and energy and water flow optimization. They propose a mixed-integer second-order cone programming (MI-SOCP) relaxation to handle the non-convex terms produced by the hydraulic characteristics of the pumps and pipes. Similarly, Mkireb et al. use mixed-integer linear programming to model variable-speed pumps to enhance the demand response and manage the uncertainties of the water demand [22]. However, it is noted that the authors of [23,24] discuss the water distribution system scheduling and operation without considering the coordination with the electrical systems. Atia and Fthenakis introduce active-salinity-control RO to enhance the integration of renewable energy and desalination loads, but they ignore the uncertainties of the demand response [16].

To minimize the total operational cost and to serve the extra wind power systems, using MI-SOCP, the authors in [25] develop a model that integrates electrical, heating, and water systems. Likewise, a model that optimally schedules water tanks and pumps was developed in [26] to collect renewable energy from the electrical grid. The model proposed in [27] optimizes the participation of RO desalination in the energy demand response and regulation markets, yet it ignores the constraints of the electrical system. A method that modifies the electric grid economic dispatch is proposed in [28] to include a water system by focusing mainly on the cogeneration of electricity and water from fossil fuel plants; however, this work ignores the network structure and other cooperation aspects. The models proposed in [25–27] investigate the potential demand response of the water network as an electric demand, yet the water production is not linked to the electrical system.

Furthermore, the work in [29] uses a robust optimization technique (ROT) to model the uncertainties in the water and electrical demands of a WEN system that mainly consists of combined water power (CWP) and single water and power energy resources. In [30], the multi-period optimization formulation includes optimal WEN in an integrated power generation and desalination systems' design and operational strategies while considering seasonal variations in water and electrical demands and fuel availability and prices. Deploying renewable energy technologies, the authors of [31] incorporated solar collectors and batteries into the same WEN's model introduced in [30] with the aim of reducing the carbon footprint. A novel optimization model is introduced for a water–energy nexus-based CHP operation to investigate the relationship between system operation optimization and water conservation [32]. Similarly, a scheduling model is proposed for the optimal operation of a combined power and desalination (CPD) system, considering MSF, RO, thermal power plants, and water storage simultaneously [33].

Based on the aforementioned discussion, it is clear that the developed WEN models lack the details needed for the design and operational variables of the integrated system. Moreover, the majority of the literature focuses heavily on the electric aspect of the system and includes minor details about the water network and the desalination processes. On

the contrary, the literature that deeply tackles various desalination processes does not link water production to the electric system. Most importantly, it is clearly noted that the existing literature ignores the network structure and other integration aspects of the cogeneration of electricity and water from thermal power plants. Also, they did not respect the flow limitations and the effort variables, such as pressure and voltage at network nodes. This work builds explicitly upon previous related works to address these aspects and considerations.

To fill the research gap in the literature, a more detailed co-optimization mathematical model for a generation-level micro-WEN system is developed, considering more variables and more complex interactions between system components. Accordingly, the proposed co-optimization model quantifies the mass and energy streams of the cogeneration plant, considering several plant variations. The proposed system focuses on attaining optimum design values and operating conditions for the micro-WEN system while minimizing the total annual and operational costs, respectively, and satisfying the electrical and water demands. Several case studies are performed to validate and evaluate the effectiveness of co-operating and co-optimizing the two systems simultaneously.

The major contributions of this paper can be summarized as follows:

- Proposing a new dynamic co-optimization framework for the design and operation of a micro-WEN system that meets the demands of the electrical and water networks at a minimum cost.
- Decoupling electricity and water production and shifting to a more sustainable water desalination technique.
- Optimizing the micro-WEN system over multiple timescales to provide solutions with a significantly smaller memory size and less computational time.

2. Problem Description

The schematic diagram of the proposed micro-WEN system is shown in Figure 2. On the electricity side of the micro-WEN system, a generation network is established and seamlessly integrated with renewable energy sources. This integration enables the system to harness the power of various renewable resources, such as solar or wind, to generate electricity. The availability of renewable energy plays a crucial role in enhancing the system's sustainability by alleviating the reliance on fossil fuels for desalination and reducing carbon emissions and environmental impact.

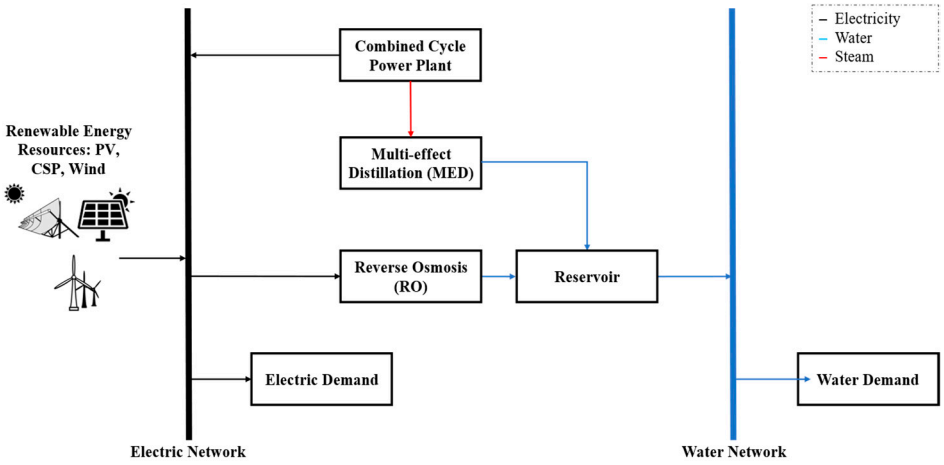

Figure 2. Physical structure of the proposed micro-WEN system.

At the core of the micro-WEN system lies a CCPP, which serves as a key power generation unit. The CCPP efficiently converts fuel into electricity using both a gas turbine and a steam turbine, maximizing energy output from the available resources. Moreover,

the waste heat produced during electricity generation is not wasted but instead redirected to the thermal desalination side of the system.

The water side of the micro-WEN system comprises a thermal desalination system, the MED, that utilizes the waste steam generated by the CCPP. In the MED process, seawater is heated in multiple evaporator stages, each operating at progressively lower pressure. The resulting vapor is condensed to produce freshwater, while the remaining brine is discharged. Additionally, to further enhance freshwater production and system flexibility, an RO desalination plant is also integrated into the water side of the micro-WEN system. The RO process involves pressurizing the feedwater against a semi-permeable membrane, separating salts and impurities from the freshwater production based on specific water source characteristics and demand patterns.

To facilitate the overall operation of the micro-WEN system, a reservoir is incorporated into the water side. Following the desalination processes, the produced freshwater is then stored in a strategically positioned reservoir. This reservoir plays a pivotal role in supplying a stable and continuous feed of freshwater to the water network, satisfying the water demand of consumers, and ensuring consistent water availability even during fluctuations in the desalination processes or water consumption patterns. While a typical water network includes pipe networks, pumps, and tanks, these elements are not explicitly considered in this work. The primary focus of the micro-WEN system is to examine the interaction and integration of the electricity generation and water desalination components, emphasizing the seamless collaboration between renewable energy utilization and sustainable freshwater production.

3. Problem Formulation

3.1. Mathematical Model of Electrical Network

In this work, a model of a power generation system is introduced. This model considers several system constraints, as follows:

- Power flow constraints: These constraints relate the active and reactive power flows in the lines to the voltages and the line impedance, as given in Equations (1) and (2). The limits of the power flow in the lines are given in Equations (3) and (4).

$$P_{ij,t} = \frac{1}{Z_{i,j}} \left(V_{i,t}^2 \cos(\theta_{ij}) - V_{i,t} V_{j,t} \cos(\delta_{i,t} - \delta_{j,t} + \theta_{ij}) \right) \tag{1}$$

$$Q_{ij,t} = \frac{1}{Z_{i,j}} \left(V_{i,t}^2 \sin(\theta_{ij}) - V_{i,t} V_{j,t} \sin(\delta_{i,t} - \delta_{j,t} + \theta_{ij}) \right) - \frac{b V_{i,t}^2}{2} \tag{2}$$

$$-P_{ij}^{max} \leq P_{ij,t} \leq P_{ij}^{max} \tag{3}$$

$$-Q_{ij}^{max} \leq Q_{ij,t} \leq Q_{ij}^{max} \tag{4}$$

- Power balance constraints: Constraint (5) illustrates the active power balance at each bus, in which the right side is the total active power flow from bus i, and the left side reflects the active power generated by generator g to bus i minus the active power demand at bus i. For several case studies, the power generation system is assumed to be integrated with a high penetration of PV resources. In this study, a probabilistic approach is adopted from [34] to model the PV system and load demand. This model utilizes historical hourly data to stimulate stochastic variations in PV output and load demand, influenced by solar irradiance and customer patterns. Also, for the transition from thermal desalination to reverse osmosis, Equation (5) accounts for the active power consumption of the water pumps in the RO system. Similarly, the reactive power balance at each bus is described by Equation (6).

$$P_{i,t}^{PV} + P_{i,t}^{g} - P_{i,t}^{L} - P_{i,t}^{RO} = \sum_{j \epsilon \Omega^i} P_{ij,t} \tag{5}$$

$$Q_{i,t}^{PV} + Q_{i,t}^{g} - Q_{i,t}^{L} - Q_{i,t}^{RO} = \sum_{j \epsilon \Omega^{i}} Q_{ij,t} \quad (6)$$

- System constraints: Several variables must be constrained within a reasonable range to ensure the stable and secure operation of the power generation system. Firstly, the voltage's magnitude and angle of each bus are constrained within a suitable voltage level, as shown in Equations (7) and (8), while Equations (9) and (10) fix the voltage's magnitude and angle of the slack bus. Also, Equations (11) and (12) set the maximum and minimum limits of power and reactive generation of generator g connected to bus *i*

$$0.9 \leq V_{i,t} \leq 1.1 \quad (7)$$

$$-\frac{\pi}{2} \leq \delta_{i,t} \leq \frac{\pi}{2} \quad (8)$$

$$V_{slack,t} = 1 \quad (9)$$

$$\delta_{slack,t} = 0 \quad (10)$$

$$P_{i}^{g,\min} \leq P_{i,t}^{g} \leq P_{i}^{g,\max} \quad (11)$$

$$Q_{i}^{g,\min} \leq Q_{i,t}^{g} \leq Q_{i}^{g,\max} \quad (12)$$

3.2. Mathematical Model of CCPP and MED

The schematic diagram of an integrated system consisting of a gas turbine, an air preheater (APH), a single-pressure heat recovery steam generator (HRSG), a steam turbine, and a MED is illustrated in Figure 3. In modeling a CCPP, some key assumptions are made to simplify its mathematical model. Firstly, the fuel used in the CCPP is methane (CH_4), and all streams operate under steady-state conditions. Additionally, air and combustion gases are treated as ideal gases with constant specific heat [35].

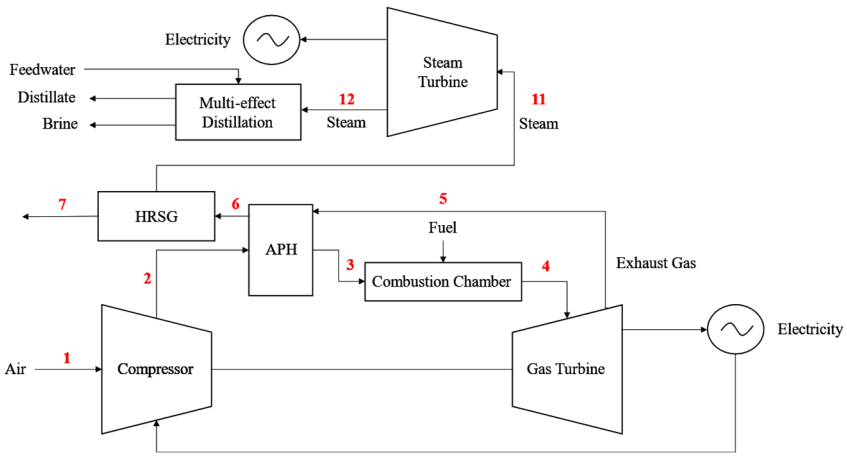

Figure 3. Schematic diagram of CCPP integrated with MED.

The mass and energy balance equations from stream 1 and stream 6 for various components of the CCPP, including the air compressor, combustion chamber, gas turbine, and APH, are described in [35,36]. The air compressor (AC) is modeled using the energy

equations given in Equations (13) and (14), where Y_a, the specific heat ratio of air, is 1.4 and $C_{p,a}$, the specific heat at constant pressure of air, is 1.004 kJ/(kgK).

$$T_2 = T_1\left(1 + \frac{1}{\eta_{AC}}\left[\left(\frac{P_2}{P_1}\right)^{\frac{Y_a-1}{Y_a}} - 1\right]\right) \tag{13}$$

$$W_{AC} = m_a\, C_{p,a}(T_2 - T_1) \tag{14}$$

The mass and energy balance equations for the combustion chamber (CC) are demonstrated in Equations (15)–(17), where LHV, the lower heating value of methane, is 50,000 kJ/kg. The mass flow rate of the air, m_a, is further expanded in Equations (18) and (19) to illustrate the combustion reaction with the molecular weights of fuel (M_f) and air (M_a).

$$m_g = m_a + m_f \tag{15}$$

$$m_a h_3 + m_f \mathrm{LHV} = m_g h_4 + m_f \mathrm{LHV}(1 - \eta_{CC}) \tag{16}$$

$$P_4 = P_3(1 - \triangle P_{CC}) \tag{17}$$

$$m_a = m_{a,rx} + m_{a,ex} \tag{18}$$

$$\frac{m_f}{M_f} = 0.5\,\frac{X_{O_2}}{M_a}\, m_{a,rx} \tag{19}$$

The mass and energy balances for the APH are identified in Equations (20)–(22), where $C_{p,g}$, the specific heat at a constant pressure of a gas, is 1.17 kJ/(kgK). Equation (22) balances the amount of energy transferred from the air to the gases in the gas turbine.

$$m_a\, C_{p,a}(T_3 - T_2) = m_g\, C_{p,g}(T_5 - T_6) \tag{20}$$

$$P_3 = P_2(1 - \triangle P_{a,APH}) \tag{21}$$

$$P_4 = P_3\left(1 - \triangle P_{g,APH}\right) \tag{22}$$

Equations (23) and (24) model the gas turbine, which generates a net power, W_{net}, by subtracting the power used to operate the AC, as shown in Equation (25). Y_g, with a value of 1.33, represents the specific heat ratio of gas. It is used to calculate the adiabatic temperature drop that would occur if the expansion in the gas turbine were isentropic.

$$T_5 = T_4\left(1 - \eta_{GT}\left[1 - \left(\frac{P_4}{P_5}\right)^{\frac{1-Y_g}{Y_g}}\right]\right) \tag{23}$$

$$W_{GT} = m_g\, C_{p,g}(T_4 - T_5) \tag{24}$$

$$W_{net} = W_{GT} - W_{AC} \tag{25}$$

Figure 4 represents the detailed schematic diagram of the HRSG and its connection with the steam turbine and the MED. The energy and mass balances for the economizer, evaporator, and superheater are given in Equations (26)–(28), respectively. Precisely, the model involves the constraints demonstrated in Equations (29)–(31) to develop the temperature profiles within the HRSG.

$$m_g\, C_{pg}\, (T_{14} - T_7) = m_s\, (h_9 - h_8) \tag{26}$$

$$m_g C_{p,g}(T_{13} - T_{14}) = m_s(h_{10} - h_9) \tag{27}$$

$$m_g C_{p,g}(T_6 - T_{13}) = m_s(h_{11} - h_{10}) \tag{28}$$

$$T_9 > T_8 \tag{29}$$

$$T_{10} = T_9 \tag{30}$$

$$T_{11} > T_{10} \tag{31}$$

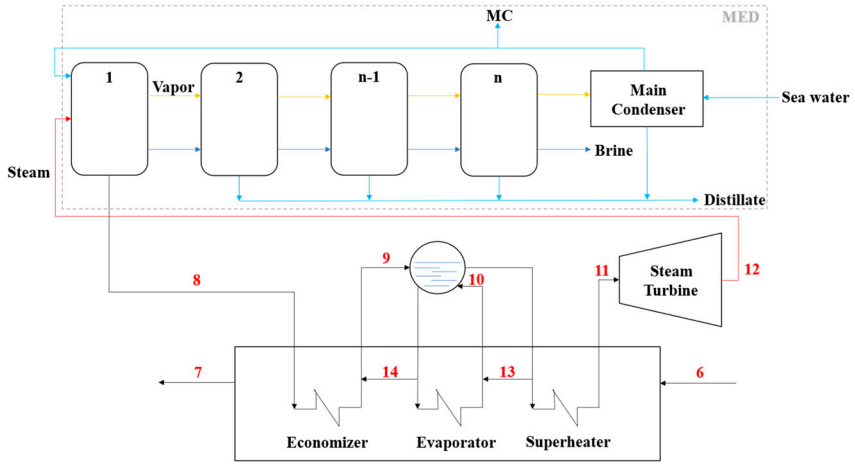

Figure 4. Schematic diagram of HRSG integrated with steam turbine and MED.

The modeling of the steam turbine mainly includes the thermodynamic properties of streams 11 and 12. Accordingly, Equation (32) indicates the power of the steam turbine [35]. Essentially, the constraint shown in Equation (33) ensures that the pressure of the steam entering the steam turbine is greater than the pressure of the steam exiting it.

$$W_{ST} = m_s\ (h_{11} - h_{12}\ )\eta_{st} \tag{32}$$

$$P_{11} > P_{12} \tag{33}$$

To model the MED system, we consider several key assumptions to derive its simplified mathematical model. The MED configuration considered here is a forward feed for simplification, although it is worth noting that the parallel/cross feed is the most energy-efficient feed configuration [37]. For this study, the MED system consists of six evaporators and a main condenser. The non-equilibrium allowance (NEA) is neglected, and the heat transfer area is constant in all effects, as presented in Equation (34). Moreover, the temperature of the seawater is at the saturation temperature of the first effect. At different temperatures and concentrations, the seawater-specific heat does not change [38,39].

$$A_{n-1} = A_n \tag{34}$$

As shown in Figure 4, the steam coming out of the steam turbine acts as a heat source for the first effect of the MED. The overall mass and energy balances of the distillation effects and the main condenser, as provided in [40], are incorporated into the mathematical model of the MED. Equations (35) and (36) ensure the overall material and salt balances for the distillation effects.

$$m_{feed}^{MED} = m_{dis} + B_{(6)} \tag{35}$$

$$X_f m_{\text{feed}} = B_{(6)} X_{\text{last}} \tag{36}$$

Equations (37)–(39) establish the mass and energy balances in the distillation effects.

$$m_{feed}^{MED} = V_{(1)} + B_{(1)} \tag{37}$$

$$V_S L_s = V_1 L_{v(1)} \tag{38}$$

$$V_{(n)} L_{v(n)} = V_n L_{v(1)} \tag{39}$$

Accordingly, Equations (40) and (41) are used to calculate the heat transfer area in the first effect and the subsequent effects. The latent heat of motive steam, L_s, and vapor, $L_{v(n)}$, are calculated using the correlation given in [40].

$$V_{(1)}L_{v(1)} = A_{(1)} \cdot U\left(T_s - T_{MED(1)}\right) \tag{40}$$

$$V_{(n)}L_{v(n)} = A_{(n)} \cdot U\left(T_{MED(n-l)} - T_{MED(n)}\right) \tag{41}$$

As mentioned earlier, Equations (42) and (43) imply that the brine acts as the feed for the next effect and calculates the brine flow rate, leaving the previous effect.

$$B_{(n-1)} = V_{(n)} + B_{(n)} \tag{42}$$

$$B_{(n-1)}X_{(n-1)} = B_{(n)}X_{(n)} \tag{43}$$

Energy balances for the main condenser are defined in Equations (44)–(46), which include the log mean temperature difference as reported in [40].

$$A_{cond} \cdot U_{cond} \cdot T_{cond} = V_{(6)}\ L_{V(6)} \tag{44}$$

$$m_{sea} \cdot C_p\left(T_{cfeed} - T_{feed}\right) = V_{(6)}L_{V(6)} \tag{45}$$

$$m_{sea} = m_c + m_{feed}^{MED} \tag{46}$$

Most importantly, the MED model incorporates the constraint given in Equation (47), which ensures that the temperature profile in effect $(\mathrm{n}-1)$ is lower than that in effect (n). Lastly, Equation (48) expresses the total MED heat transfer area.

$$T_{MED(n-1)} > T_{MED(n)} \tag{47}$$

$$HTA_{MED} = A_{cond} + \sum_{1}^{n} A_{(n)} \tag{48}$$

3.3. Mathematical Model of RO Desalination

In this work, the RO is a single-stage desalination system consisting of six parallel vessels, each comprising six membranes. Mainly, the RO system consists of a high-pressure pumping unit that consumes a significant amount of electricity. A simple mathematical model describing the RO desalination process is derived from references [31,41]. Equation (49) provides an estimate of the specific power consumption of the high-pressure pumping unit, with the seawater's density, ρ, assumed to be $1060\,\frac{\mathrm{kg}}{\mathrm{m}^3}$.

$$W_{RO} = \frac{n_{RO}\ P_{h,f}\ m_{feed}^{RO}}{\eta_{RO}\ \rho^s} \tag{49}$$

3.4. Mathematical Model of Reservoir

In this work, a lumped approach is employed to consider the distillate production from the MED system as uniform at all times, facilitating the development of a simplified and fast model. Equation (50) ensures that the water demand at the current hour is fulfilled by the distillate, which is added to the difference between the reservoir capacity at the previous and current hours. As illustrated in Equation (50), a factor of 3.6 is added to convert the distillate flow rate from kg/s to m^3/h. Equation (51) applies the exact correlation, but with the initial capacity of the reservoir at the first hour. Most importantly, to demonstrate a

complete cycle, the reservoir's capacity at the end of the current day should be nearly equal to its capacity at the beginning of the next day, i.e., $W_{res(24)} = W_{res(1)}$.

$$3.6\, m_{dis} + W_{res(t-1)} = W_{res(t)} + W_{demand(t)} \quad (50)$$

$$3.6\, m_{dis} + W_{res(24)} = W_{res(1)} + W_{demand(1)} \quad (51)$$

3.5. Integration of Power and Water Systems

In the proposed micro-WEN system, the co-optimization of electrical power and water networks occurs in two stages. The first stage involves the integration of the CCPP and the MED systems, while the second stage includes the integration of the CCPP, the MED, and the power generation network.

As elaborated in previous sections, the steam exiting the steam turbine serves as the heat source for the first effect of the MED. This relationship is incorporated as a constraint in the integrated micro-WEN model, as expressed in Equations (52)–(55).

$$m_s = V_s \quad (52)$$

$$T_{12} = T_s \quad (53)$$

$$T_{12} = T_8 \quad (54)$$

$$60 \leq\ T_s \leq 110 \quad (55)$$

To integrate the CCPP with the IEEE 24-bus system, the total generated power from the gas and steam turbines is injected into the buses where the cogeneration units are installed. Given that the CCPP model operates on a daily scale while the electrical network is time-based, the output power of the CCPP at bus i is represented as the daily average generated power, as given in Equation (56).

$$\sum_{t=1}^{24} P_{i,t}^{g} = W_{net} + W_{ST} \quad (56)$$

3.6. Economic Models

To assess the cost of the proposed micro-WEN system, the economic model of the CCPP is obtained from previous studies [35,42,43]. It is vital to account for the annual fuel cost used in the CCPP, the capital investment, and the maintenance costs. Equation (57) estimates the total annual cost of the CCPP, which comprises the total fuel cost, where c_f represents the fuel cost per energy unit, with a value of 0.004 USD/MJ and the purchase costs (Z) of AC, APH, CC, GT, HRSG, APH, and ST. In Equation (57), N_{CCPP} corresponds to the total number of operating hours per year, which is 8000 h. Additionally, CRF represents the yearly capital recovery factor at a rate of 18.2%, and the maintenance factor (MF) is set to 1.06.

$$TAC_{CCPP} = 3600\, N_{CCPP}\, c_f m_f LHV + CRF\, MF\, (Z_{AC} + Z_{CC} + Z_{GT} + Z_{HRSG} + Z_{APH} + Z_{ST}) \quad (57)$$

Details on modeling the MED's economic performance are obtained from the recent literature [39,40]. The total annual cost of the MED system takes into account both the total annual capital and operating costs, as demonstrated in Equation (58). The total annual investment cost (TAC_{MED}) comprises equipment and civil work capital costs, while the annual operating cost evaluates the costs of electric power, steam, labor, maintenance, and insurance.

$$TAC_{MED} = CRF\, TCC_{MED} + AOC_{MED} \quad (58)$$

3.7. Proposed Approach: Optimal Design of a Micro-WEN System

The proposed micro-WEN system is co-optimized as an integrated physical system to minimize its total annual cost and meet daily electricity and water demands. The optimization model is defined below.

$$\left.\begin{array}{c} min\ TAC_{\ WEN} = TAC_{CCPP} + TAC_{MED} \\ \\ Subject\ to \\ \\ Mathematical\ models\ of\ electrical\ network,\ CCPP,\ MED,\ and\ reservoir \\ Integration\ of\ power\ and\ water\ systems \\ Economic\ models \end{array}\right\}$$

3.8. Proposed Approach: Optimal Operation of a Micro-WEN System with RO

The proposed micro-WEN system that incorporates RO desalination instead of MED is co-optimized to minimize its total operational cost, as presented below. The 24 h electricity price at the power transmission bus is represented by p_e.

$$\left.\begin{array}{c} min\ OC_{\ WEN} = \sum\limits_{i,\,t} b_g\ P^g_{i,t}\ S_{base} + \sum\limits_{t} p_e W_{RO} \\ \\ Subject\ to \\ \\ Mathematical\ models\ of\ electrical\ network,\ RO,\ and\ reservoir \\ Integration\ of\ PV\ system\ and\ electrical\ network \end{array}\right\}$$

4. Results and Discussions

This section discusses the simulation results of the proposed approach, which was tested using the IEEE 24-bus generation system, as shown in Figure 5. The system includes 24 nodes, 24 thermal units, and 38 transmission lines. The capacity of the IEEE 24-bus system is 2890 MW, with a maximum demand of 2850 MW, as shown in Figure 6, illustrating the generated power at each bus.

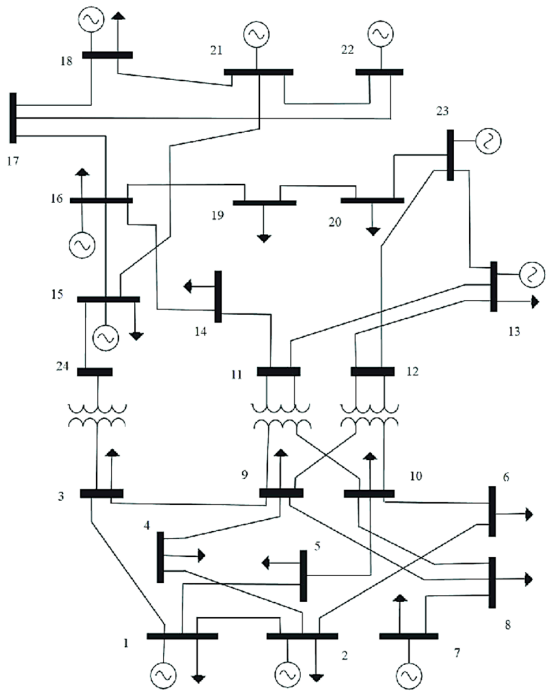

Figure 5. IEEE 24-bus system [44].

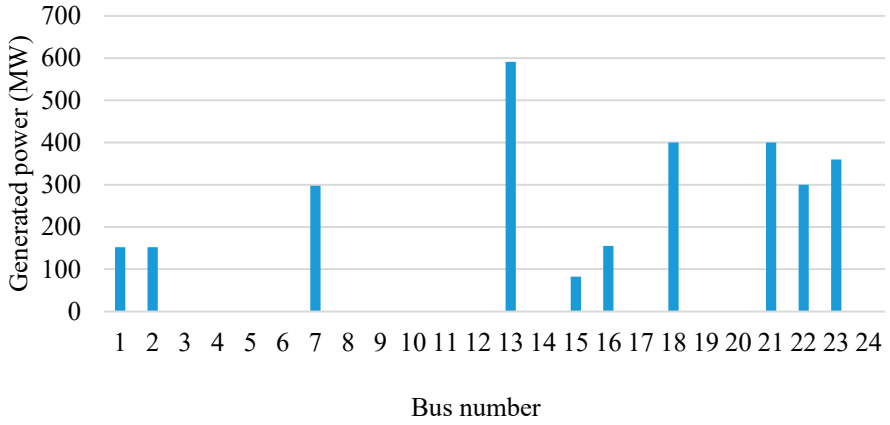

Figure 6. Generated peak power at each bus of the IEEE 24-bus system.

Two possible approaches are introduced to optimize the design and operation of the proposed micro-WEN system based on the previously discussed mathematical models. First, for optimal design, we minimize the total annual cost of the developed micro-WEN system by co-optimizing the design of the CCPP and MED systems while meeting the daily electrical and water demands. Secondly, shifting to RO, the proposed micro-WEN system is co-optimized to achieve the minimum total operational cost, both with and without a PV system, for optimal system operation. The NLP optimization models and solving approaches are implemented in the GAMS modeling environment and solved using the CONOPT solver.

4.1. Performance Evaluation of Proposed Approach

Before optimization, model variables in the following model are initialized to values in recent related works to acquire feasible initial solutions that satisfy mass and energy balances in each component of the MED system and the CCPP. In the development of the simulation model, no objective function is initially considered. Instead, the feasible solution obtained for the model is used as an initialization point for minimizing the total annual cost of the micro-WEN system. The model variables for the CCPP and MED systems are bounded by lower and upper bounds from the recent related literature, as listed in Table 1.

Table 1. Lower and upper bounds of operating conditions of the micro-WEN system.

Operating Conditions		Lower Bounds	Upper Bounds
MED	T_{cfeed}	30 °C	80 °C
	$T_{MED(n)}$	36 °C	130 °C
	$L_{v(n)}$	2000 kJ/kg	3000 kJ/kg
	T_s	80 °C	150 °C
CCPP	W_{net}	30 MW	-
	W_{ST}	11 MW	-
	T_k	298.15 K	1500 K
	m_a	94 kg/s	-

Applying the co-optimization approach, Table 2 summarizes the optimal design values of the MED system and the CCPP that meet typical daily electrical and water load demands. The optimal operating conditions of all flows, such as mass flow rates, temperature, and pressure, are summarized in Table 3. Most importantly, the results in Tables 2 and 3 strongly align with findings in the existing literature and previous works, confirming the feasibility of the proposed approach.

Table 2. Optimum values of design variables of the micro-WEN system.

Design Variables		Value
MED	n_{MED}	6
	HTA_{MED}	5985 m^2
CCPP	η_{GT}	54.9%
	η_{ST}	96.5%
	W	150 MW

Table 3. Optimum values of operating conditions of the micro-WEN system.

Operating Conditions		Value
MED	m_{feed}^{MED}	136.65 kg/s
	V_s	63.193 kg/s
	m_{dis}	40.41 kg/s
	T_s	110 °C
CCPP	m_s	6.42 kg/s
	m_f	0.601 kg/s
	m_a	41.86 kg/s
	T_{12}	383.15 K
	P_{11}	1.101 bar
	P_{12}	0.101 bar

The optimal distribution between the capital investment and operating costs, leading to the minimal total annual cost of the micro-WEN system, is presented in Table 4, with 'M' denoting millions. The simultaneous co-optimization of both power and water aspects in the micro-WEN system offers a significant advantage. The observed reduction in computational time and cost, compared to independent optimization approaches typically used in the literature, showcases the efficiency and practicality of the proposed co-optimization approach.

Table 4. Capital investment and operating costs of the micro-WEN system.

System	Capital Investment (USD/year)	Operating Cost (USD/year)
MED	1.82 M	1.12 M
CCPP	0.86 M	3.5 M
Micro-WEN	5.91 M	

To meet the demand in both the energy and water sectors, the cogeneration unit is designed with capacities of 145 m^3/h for water and 150 MW for electricity. Maintaining the same design specifications and operating conditions of the micro-WEN system, different case studies are investigated to estimate the number of cogeneration units needed to replace the generating units in the IEEE 24-bus system. These studies consider different percentages of the electricity consumed by the residential sector. According to [45], UAE residents typically use approximately 0.55 m^3 of water and 25 kWh of electricity per day.

In the UAE, the consumption of the residential sector in Abu Dhabi constitutes 26.8% of the total consumption [46]. Considering 26.8%, 50%, and 100% of the residential electricity consumption, Table 5 summarizes the number of households that the electrical system can serve, their daily water consumption, and the corresponding number of cogeneration units meeting the water consumption needs. As shown in Table 5, five cogeneration units totaling 750 MW capacity are needed to meet the water demand of 30,984 households. Consequently, as shown in Figure 7, the generating units at buses 15, 22, and 23, with capacities of 82 MW, 300 MW, and 360 MW, respectively, are replaced by five cogeneration units located at buses 5, 15, 19, 22, and 23.

Table 5. Various percentages of electricity consumption by the residential sector.

Residential Sector Percentage	No. of Households	Daily Water Consumption (m^3/day)	No. of Cogeneration Units
26.8%	30,984	17,041.2	5
50%	57,806	31,793.3	17
100%	115,612	63,538.6	20

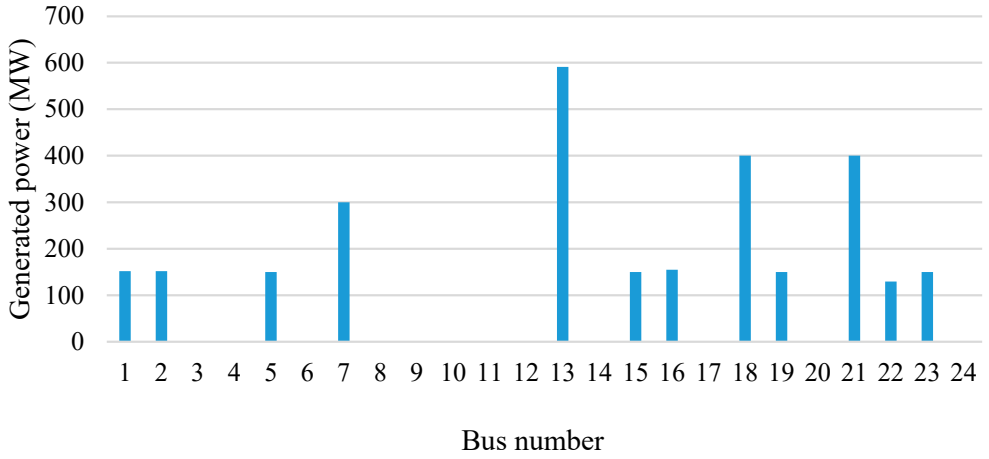

Figure 7. Generated power at each bus with five cogeneration units.

An increase in the number of households leads to a proportional increase in the required number of cogeneration units to meet the daily water demand. Thus, to meet the water demand of 57,806 households at 31,793.3 m^3/day, seventeen cogeneration units are required. Consequently, as shown in Figure 8, seventeen cogeneration units are added, replacing all generating units of the IEEE 24-bus system except for the generator at bus 23.

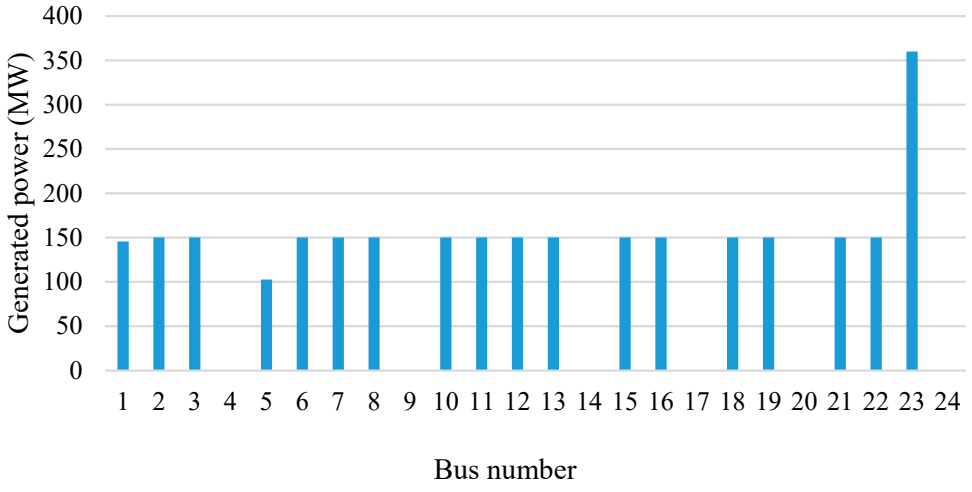

Figure 8. Generated power at each bus with seventeen cogeneration units.

To satisfy the electrical and water demands of an area comprising only the residential sector, twenty cogeneration units are installed, replacing all the generating units in the electrical network. Their locations are indicated in Figure 9.

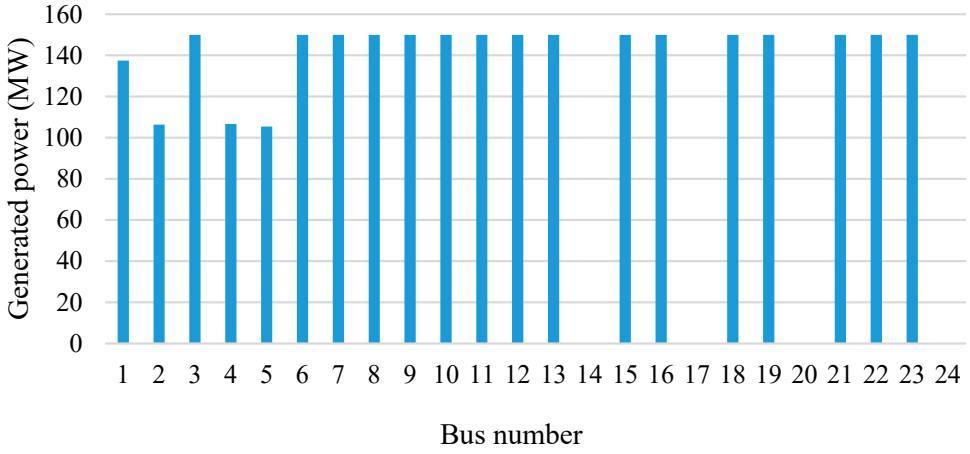

Figure 9. Generated power at each bus with twenty cogeneration units.

4.2. Effect of PV Integration

This subsection discusses the integration of a renewable energy resource into the generation network to assess its impact on meeting the electrical and water demands that the cogeneration unit should fulfill. Therefore, a 50 MW PV system is incorporated into the proposed micro-WEN system, located at bus 17.

To compare the 26.8% variation in the generated power at each bus before and after integrating the PV system into the proposed micro-WEN system serving households, Figures 10 and 11 represent the hourly generated power at each bus and the hourly output power of the PV system, respectively.

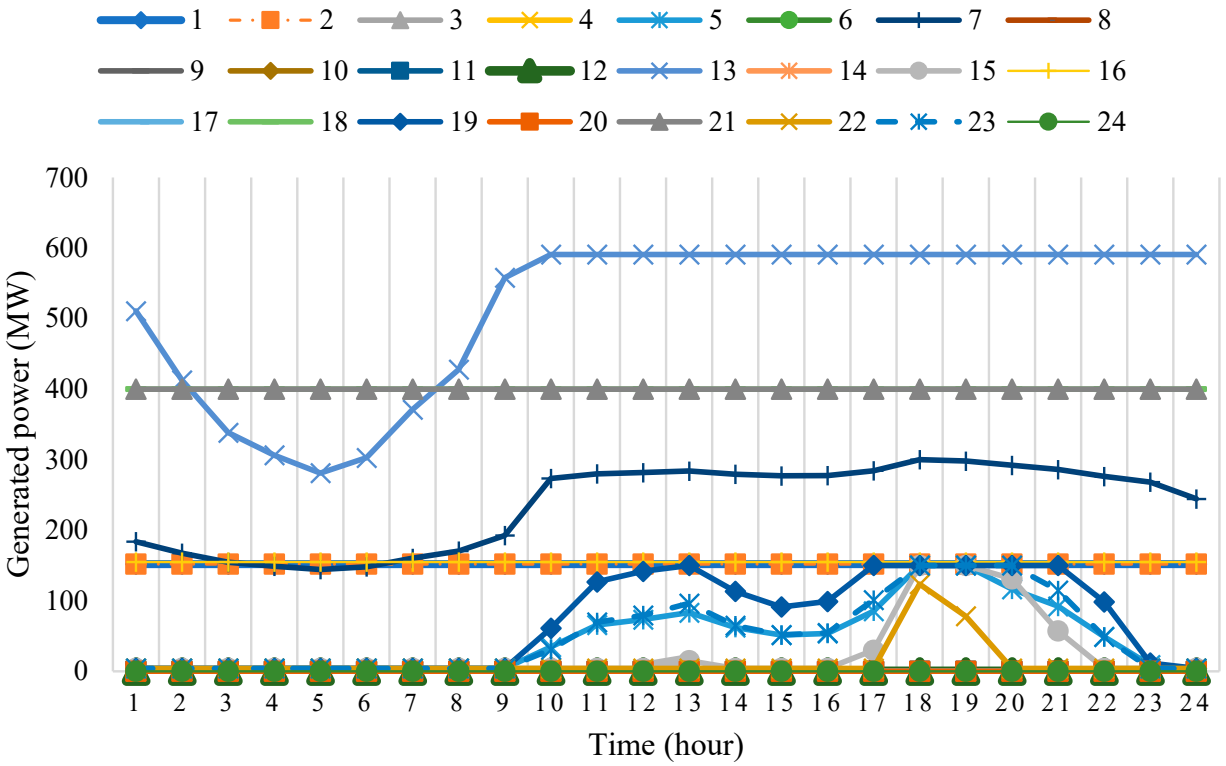

Figure 10. Hourly generated power at each bus with PV system.

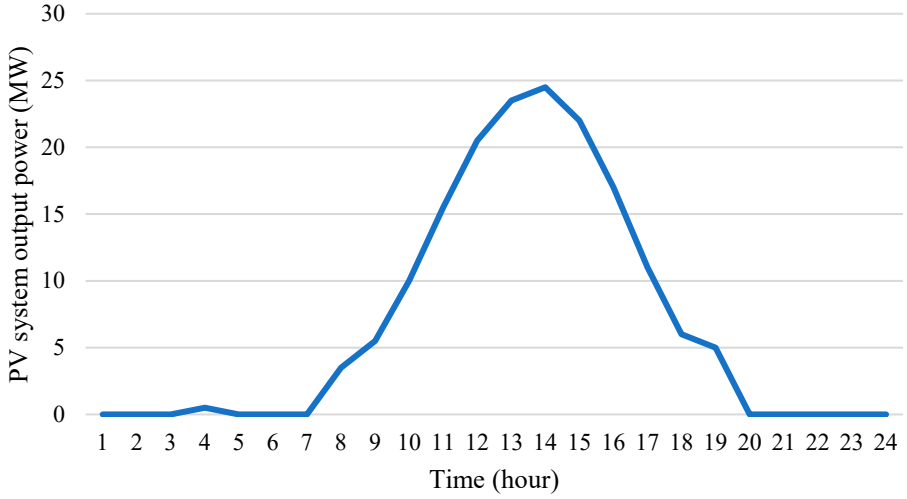

Figure 11. Hourly output power of PV system.

As presumed, with the addition of the PV system, it can be inferred that the generated power at the buses hosting the cogeneration units decreases between 9:00 am and 5:00 pm when the PV system supplies power to the electrical network. If a PV system of sufficient size generates the same amount of electricity as a cogeneration unit, it can lead to the shutdown of the cogeneration unit. In such a scenario, the freshwater produced by the cogeneration units may not meet the water demand. To address this problem, we propose decoupling electricity and water production by gradually phasing out the cogeneration units and shifting to the reverse osmosis desalination technique.

4.3. Shifting to Reverse Osmosis (RO)

As previously discussed, if another source supplies the same amount of electricity that the cogeneration unit generates, it can result in its shutdown. In that case, the freshwater produced by the cogeneration units will not meet the water demand. Thus, this work proposes to shift to more sustainable water desalination and decouple electricity and water production. The best approach is to shift from thermal desalination, which consumes a significant amount of electricity, to RO. Nevertheless, any renewable energy resource, such as a PV system or a storage system like a battery, may provide this electricity to produce water. As a result, water desalination will not rely on thermal energy from the CCPP.

The optimization model defined in (60), incorporating a simple mathematical model of the RO desalination process reported in [31,41], is employed to obtain the optimal design values for an RO system that meets a typical daily water demand at a minimum cost. The corresponding values are reported in Table 6. The reservoir has an initial capacity of 190.25 m^3 and is supplied hourly with a constant permeate of 145.48 m^3. Consequently, as shown in Figure 12, the RO system satisfies the water demand regardless of whether it is integrated with a PV system or cogeneration units.

Table 6. Optimal values of design variables of the RO system.

Design Variables		Value
RO	n_{RO}	36
	A_{RO}	197.88 m^2

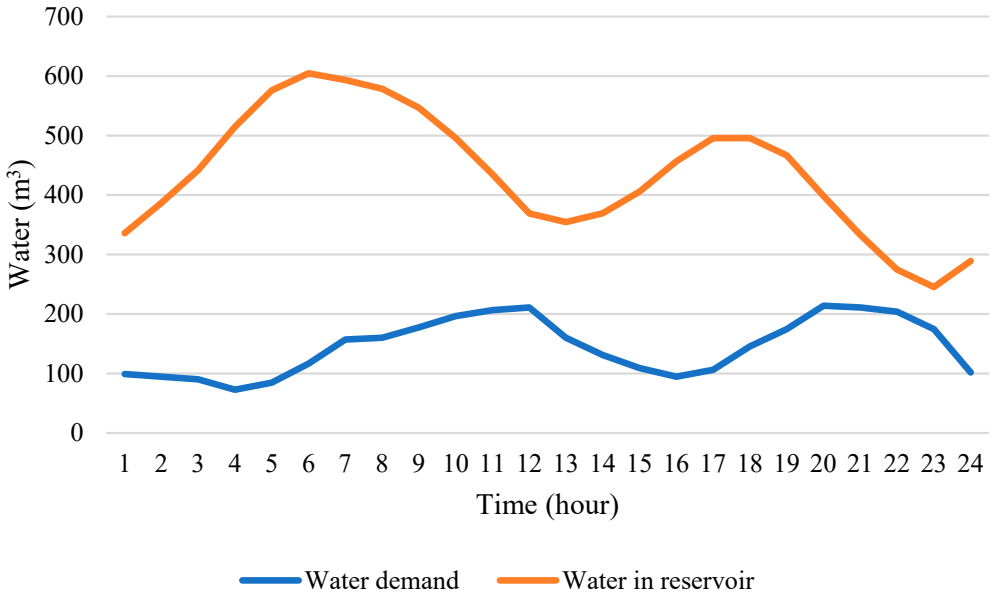

Figure 12. Water demand vs. water in the reservoir.

This work considers seasonal variations as the electricity demand varies depending on the season. It displays the year as four days, for a total of 96 h slots, where each day represents a season and constitutes 24 h slots. The normalized electrical demand of each season sample day is shown in Figure 13. Also, Figure 14 presents the hourly output power of the PV system across different seasons—winter, spring, summer, and autumn. It is evident that the output power of the PV system reflects the fluctuations in solar irradiance. The water pump consumes 887.144 kWh of electricity and pumps feed at a rate of 362.75 m^3/h to meet the water demand. On that account, considering a unity power factor, the reactive power is compensated in the water pumps of the RO system.

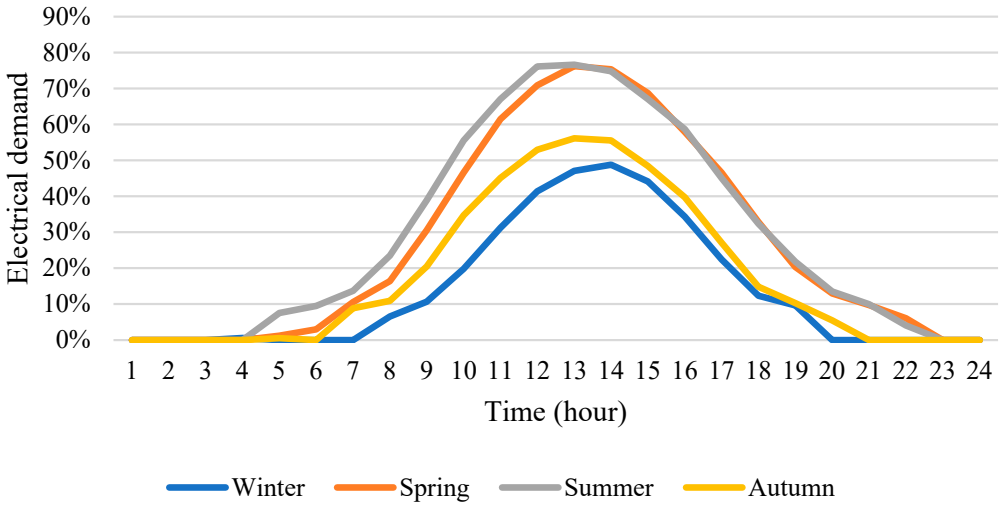

Figure 13. Seasonal electric demand.

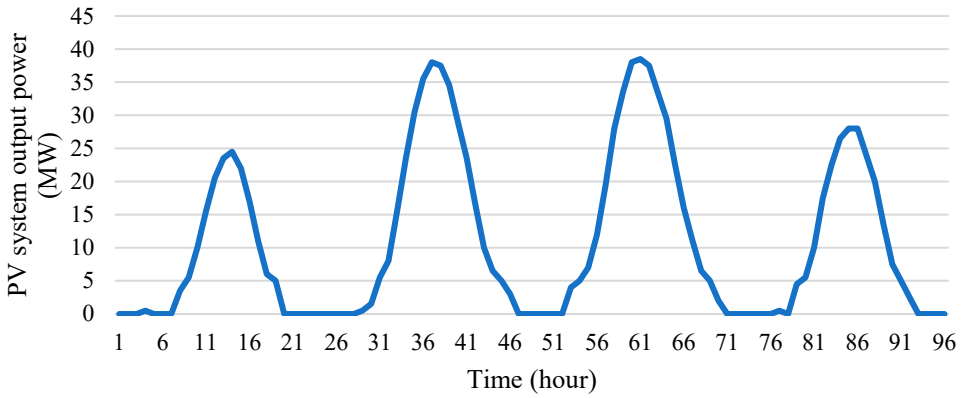

Figure 14. Hourly output power of PV system across four seasons.

The addition of the water pump at bus 7 initially boosts power generation, but the subsequent inclusion of a PV system reduces it as the PV system contributes extra active power to the electrical network, as shown in Figure 15.

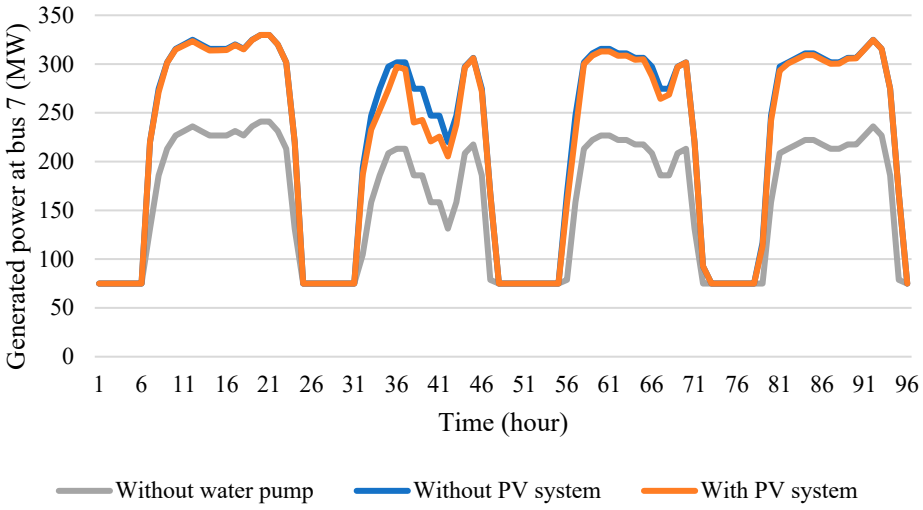

Figure 15. Hourly generated power at bus 7.

4.4. Optimal Operation of a Micro-WEN System with RO

As summarized in Table 7, the proposed co-optimization model in (60) yields the optimal operating conditions for the RO system using the mathematical model of the RO desalination process that is presented in [31,41].

Table 7. Optimal values of operating conditions for the RO system.

Operating Conditions		Value
RO	m_{feed}^{RO}	2.8 kg/s
	m_b	1.68 kg/s
	m_p	1.12 kg/s
	SR	99.6%

Table 8 highlights the minimum operating cost of the proposed micro-WEN system, both without and with a PV system. Also, the total operating cost of the micro-WEN, with the RO system replacing the cogeneration units to satisfy the water demand, is defined. As a result, according to Table 8, co-optimizing the overall system with PV saves approximately USD 0.01 M, and shifting from the cogeneration units to the RO system results in a 26.7% reduction in the total operational cost of the proposed micro-WEN system.

Table 8. Comparison of total operating cost of micro-WEN system.

Operating Conditions	Total Operating Cost (USD/Day)
Without PV	0.82 M
With PV	0.81 M
Shifting to RO	0.61 M

5. Conclusions

Efficiently managing water–energy nexus systems is essential to meet the growing demand for water and electricity. The integration of seawater thermal desalination into a combined-cycle power generation plant offers a promising solution for both power generation and water desalination. To achieve optimal performance, it is crucial to implement innovative and robust resource management strategies aimed at reducing the total operational cost of micro-WEN systems while maximizing the utilization of the available energy resources. In this paper, we propose an NLP mathematical model for micro-WEN systems at the generation level, incorporating a co-optimization framework for their design and operation. This approach aims to fulfill the requirements of both the electrical and water networks at the lowest possible cost. Our research specifically addresses the challenge faced by power plants in the United Arab Emirates, which operate at reduced efficiency during the winter season in order to meet water demand. This challenge is addressed by transitioning from thermal desalination to reverse osmosis desalination and decoupling the production of energy and water. The results demonstrate a significant reduction in overall operational costs of 26.7% through the transition to RO desalination. By optimizing the micro-WEN system at various timescales, including hourly and daily intervals, we offer solutions that not only require less memory but also reduce computational time.

While the current study focuses on optimizing the integration of water and energy systems through dynamic co-optimization approaches, the integration of photovoltaic energy storage technologies presents a promising enhancement to the sustainability and efficiency of micro-WEN systems. Energy storage can provide crucial support in balancing the fluctuations in solar energy generation, thus ensuring a more reliable and steady energy supply to the integrated systems. Future research could explore how different energy storage technologies can be effectively incorporated into the water–energy nexus to enhance operational flexibility and energy security. Moreover, future studies are recommended to develop a scaling approach for integrated water–energy systems, incorporating projections for the expansion of installed renewable energy capacities. This development should include the formulation of a trend function characterized by an annual growth rate of installed power. Such a methodology would facilitate strategic planning and optimization of system expansions over time, aligning with global trends in renewable energy development. Additionally, it would support strategic planning and policy formulation aimed at sustainable energy and water management.

Author Contributions: Conceptualization, M.E., M.F.S. and A.O.; methodology, M.E. and M.F.S.; software, M.E., A.A. and A.P.; validation, M.K., A.A. and A.O.; formal analysis, M.E., A.P. and A.A.; investigation, A.O. and M.K.; resources, M.F.S. and A.O.; data curation, M.E. and A.P.; writing—original draft preparation, M.E.; writing—review and editing, M.F.S., A.O. and A.A.; visualization, M.K. and A.A.; supervision, M.F.S., A.O. and M.K.; project administration, M.F.S. and A.O.; funding acquisition, M.F.S. and A.O. All authors have read and agreed to the published version of the manuscript.

Funding: The work in this paper was supported, in part, by project FRG22-C-E24 and the Open Access Program from the American University of Sharjah. This paper represents the opinions of the authors and does not mean to represent the position or opinions of the American University of Sharjah.

Institutional Review Board Statement: Not applicable.

Informed Consent Statement: Not applicable.

Data Availability Statement: No new data were created or analyzed in this study.

Conflicts of Interest: The authors declare no conflicts of interest.

Nomenclature

g	index of generators	T_{feed}	intake seawater temperature, °C
i, j	index of buses in the electrical network	U	overall heat transfer coefficients, kW/(m^2 °C)
k	index of streams in CCPP	$W_{demand\ (t)}$	water demand at time t, m^3/h
n	number of distillation effects in MED	X_{O2}	molar fraction of oxygen
t	index of time periods	X_b	salt concentration in brine, ppm
b_g	fuel cost coefficient of generator g	X_f	salt concentration in feed seawater, ppm
C_e	electricity cost, USD/kWh	γ_a	specific heat ratio of air
C_f	fuel cost, USD/MJ	Z_{ij}	impedance of branch ij
$C_{p,a}$	specific heat at a constant pressure of air	$\triangle P_{CC}$	pressure difference in the combustion chamber
CRF	capital recovery factor	$\triangle TLM$	log mean temperature difference
LHV	lower heating value, kJ/kg	θ_{ij}	phase angle of the impedance of branch ij
M_f	molecular weight of fuel	A_n	heat transfer surface area in effect n, m^2
MF	maintenance factor	AOC	annual operational cost
N_{CCPP}	annual operation time of CCPP, h/year	B_n	brine flow rate in effect n of MED, kg/s
n_{RO}	number of membranes in RO	h_k	specific enthalpy of stream k, kJ/kg
η_{CC}	first-law efficiency of the combustion chamber	HTA_{MED}	total heat transfer surface area of MED, m$_2$
$P^L{}_{i,t}$	active power load of bus i at time t, MW	L_s	latent heat of motive steam, kJ/kg
$P_i{}^{g,max}$	maximum limit of active power output of g connected to bus i	$L_{v\ (n)}$	latent heat in effect n, kJ/kg
$P_i{}^{g,min}$	minimum limit of active power output of g connected to bus i	m_a	air mass flow rate, kg/s
$P_{ij}{}^{max}$	maximum limit of active power flow of branch ij	m_c	exit water to sea from main condenser, kg/s
ρ^s	average density of seawater, kg/m^3	m_{dis}	net distillate produced from MED, kg/s
$Q^L{}_{i,t}$	reactive power load of bus i at time t, MW	m_f	fuel mass flow rate, kg/s
$Q_i{}^{g,max}$	maximum limit of reactive power output of g connected to bus i	$m_{feed}{}^{MED}$	feed water flow rate at first effect in MED, kg/s
$Q_i{}^{g,min}$	minimum limit of reactive power output of g connected to bus i	$m_{feed}{}^{RO}$	feed water flow rate in RO, kg/s
$Q_{ij}{}^{max}$	maximum limit of reactive power flow of branch ij	m_g	combustion gases mass flow rate, kg/s
		m_s	steam mass flow rate, kg/s

References

1. United States Department of Energy. The Water-Energy Nexus: Challenges and Opportunities Overview and Summary. 2014. Available online: https://www.google.com/url?sa=t&source=web&rct=j&opi=89978449&url=https://www.energy.gov/sites/prod/files/2014/07/f17/Water%2520Energy%2520Nexus%2520Full%2520Report%2520July%25202014.pdf&ved=2ahUKEwiF6vOcjNiFAxVHlFYBHQk6A0oQFnoECBMQAQ&usg=AOvVaw1gEgkAs04DkYicMdp_HeGv (accessed on 14 December 2023).
2. Olsson, G. *Water and Energy*; IWA Publishing: London, UK, 2015; ISBN 9781780406947.
3. Siddiqi, A.; Anadon, L.D. The water-energy nexus in Middle East and North Africa. *Energy Policy* **2011**, *39*, 4529–4540. [CrossRef]
4. Peterson, J.M. Water-Energy-Food Nexus-Commonalities and Differences in the United States and Europe. In *Competition for Water Resources Experiences and Management Approaches in the US and Europe*; Elsevier: Amsterdam, The Netherlands, 2017; pp. 252–258. [CrossRef]
5. IRENA. Renewable energy in the water, energy and food nexus. In *International Renewable Energy Agency*; IRENA: Abu Dhabi, United Arab Emirates, 2015; pp. 1–125.
6. Elsaid, K.; Kamil, M.; Sayed, E.T.; Abdelkareem, M.A.; Wilberforce, T.; Olabi, A. Environmental impact of desalination technologies: A review. *Sci. Total Environ.* **2020**, *748*, 141528. [CrossRef] [PubMed]
7. West, W. In the Water and Energy Nexus: A Literature Review. 2013. Available online: https://waterinthewest.stanford.edu/sites/default/files/Water-Energy_Lit_Review.pdf (accessed on 16 December 2023).
8. El-Halwagi, M.M. *Water–Energy Nexus for Thermal Desalination Processes*; Elsevier: Amsterdam, The Netherlands, 2017; ISBN 9780128098233.
9. Inayat, A.; Raza, M. District cooling system via renewable energy sources: A review. *Renew. Sustain. Energy Rev.* **2019**, *107*, 360–373. [CrossRef]

10. Çakir, U.; Çomakli, K.; Yüksel, F. The role of cogeneration systems in sustainability of energy. *Energy Convers. Manag.* **2012**, *63*, 196–202. [CrossRef]
11. Breeze, P. *Gas-Turbine Power Generation*; Elsevier: Amsterdam, The Netherlands, 2016; ISBN 9780128040058.
12. Harandi, H.B.; Asadi, A.; Rahnama, M.; Shen, Z.G.; Sui, P.C. Modeling and multi-objective optimization of integrated MED–TVC desalination system and gas power plant for waste heat harvesting. *Comput. Chem. Eng.* **2021**, *149*, 107294. [CrossRef]
13. Aklilu, B.T.; Gilani, S.I. Mathematical modeling and simulation of a cogeneration plant. *Appl. Therm. Eng.* **2010**, *30*, 2545–2554. [CrossRef]
14. IRENA. Water Desalination Using Renewable Energy. 2012. Available online: www.etsap.org-www.irena.org (accessed on 14 December 2023).
15. Mehrjerdi, H. Modeling and optimization of an island water-energy nexus powered by a hybrid solar-wind renewable system. *Energy* **2020**, *197*, 117217. [CrossRef]
16. Alnahhal, Z.H.; Shaaban, M.F.; Hamouda, M.; Mokhtar, M. Optimal Operation of Power System Integrated with Reverse Osmosis Water Desalination. In Proceedings of the 2021 6th International Symposium on Environment-Friendly Energies and Applications (EFEA), Sofia, Bulgaria, 24–26 March 2021; pp. 6–10. [CrossRef]
17. Wang, C.; Gao, N.; Wang, J.; Jia, N.; Bi, T.; Martin, K. Robust Operation of a Water-Energy Nexus: A Multi-Energy Perspective. *IEEE Trans. Sustain. Energy* **2020**, *11*, 2698–2712. [CrossRef]
18. Moazeni, F.; Khazaei, J. Co-optimization of wastewater treatment plants interconnected with smart grids. *Appl. Energy* **2021**, *298*, 117150. [CrossRef]
19. Mohammadi, F.; Sahraei-Ardakani, M.; Al-Abdullah, Y.M.; Heydt, G.T. Coordinated Scheduling of Power Generation and Water Desalination Units. *IEEE Trans. Power Syst.* **2019**, *34*, 3657–3666. [CrossRef]
20. Tayerani Charmchi, A.S.; Ifaei, P.; Yoo, C.K. Smart supply-side management of optimal hydro reservoirs using the water/energy nexus concept: A hydropower pinch analysis. *Appl. Energy* **2021**, *281*, 116136. [CrossRef]
21. Fooladivanda, D.; Taylor, J.A. Energy-optimal pump scheduling and water flow. *IEEE Trans. Control Netw. Syst.* **2018**, *5*, 1016–1026. [CrossRef]
22. Mkireb, C.; Dembélé, A.; Jouglet, A.; Denoeux, T. Robust Optimization of Demand Response Power Bids for Drinking Water Systems. *Appl. Energy* **2019**, *238*, 1036–1047. [CrossRef]
23. Atia, A.A.; Fthenakis, V. Active-salinity-control reverse osmosis desalination as a flexible load resource. *Desalination* **2019**, *468*, 114062. [CrossRef]
24. Menke, R.; Abraham, E.; Parpas, P.; Stoianov, I. Extending the Envelope of Demand Response Provision though Variable Speed Pumps. *Procedia Eng.* **2017**, *186*, 584–591. [CrossRef]
25. Li, C.; Yao, Y.; Xie, K.; Hu, B.; Niu, T. Integrated Electrical, Heating, and Water Distribution System to Accommodate Wind Power. *IEEE Trans. Sustain. Energy* **2021**, *12*, 1100–1114. [CrossRef]
26. Fooladivanda, D.; Dominguez-Garcia, A.D.; Sauer, P.W. Utilization of Water Supply Networks for Harvesting Renewable Energy. *IEEE Trans. Control Netw. Syst.* **2019**, *6*, 763–774. [CrossRef]
27. Oikonomou, K.; Parvania, M. Optimal Participation of Water Desalination Plants in Electricity Demand Response and Regulation Markets. *IEEE Syst. J.* **2020**, *14*, 3729–3739. [CrossRef]
28. Santhosh, A.; Farid, A.M.; Youcef-Toumi, K. Real-time economic dispatch for the supply side of the energy-water nexus. *Appl. Energy* **2014**, *122*, 42–52. [CrossRef]
29. Guo, Q.; Guo, T.; Tian, Q.; Nojavan, S. Optimal robust scheduling of energy-water nexus system using robust optimization technique. *Comput. Chem. Eng.* **2021**, *155*, 107542. [CrossRef]
30. Al-Fadhli, F.M.; Alhajeri, N.; Ettouney, H.; Sengupta, D.; Holtzapple, M.; El-Halwagi, M.M. Simultaneous optimization of power generation and desalination systems: A general approach with applications to Kuwait. *Clean Technol. Environ. Policy* **2022**, *24*, 2129–2141. [CrossRef]
31. Al-Fadhli, F.M.; Alhajeri, N.S.; Sholapurmath, R.; Ettouney, H.; Sengupta, D.; Holtzapple, M.; El-Halwagi, M.M. Optimizing cogeneration and desalination plants by incorporating solar energy. *Desalination* **2023**, *549*, 116320. [CrossRef]
32. Wang, S.; Wang, X.; Fu, Z.; Liu, F.; Xu, Y.; Li, W. A novel energy-water nexus based CHP operation optimization model under water shortage. *Energy* **2022**, *239*, 121832. [CrossRef]
33. Xiao, S.; Guan, Q.; Zhang, W.; Wu, L. Optimal scheduling of the combined power and desalination system. *Energy Rep.* **2022**, *8*, 661–669. [CrossRef]
34. Oda, E.S.; Abd El Hamed, A.M.; Ali, A.; Elbaset, A.A.; El Sattar, M.A.; Ebeed, M. Stochastic optimal planning of distribution system considering integrated photovoltaic-based dg and dstatcom under uncertainties of loads and solar irradiance. *IEEE Access* **2021**, *9*, 26541–26555. [CrossRef]
35. Valero, A.; Lozano, M.A.; Serra, L.; Tsatsaronis, G.; Pisa, J.; Frangopoulos, C.; von Spakovsky, M.R. CGAM problem: Definition and conventional solution. *Energy* **1994**, *19*, 279–286. [CrossRef]
36. Hanafi, A.S.; Mostafa, G.M.; Fathy, A.; Waheed, A. Thermo-Economic Analysis of Combined Cycle MED-TVC Desalination System. *Energy Procedia* **2015**, *75*, 1005–1020. [CrossRef]
37. Sharan, P.; Neises, T.; Turchi, C. Optimal feed flow sequence for multi-effect distillation system integrated with supercritical carbon dioxide Brayton cycle for seawater desalination. *J. Clean. Prod.* **2018**, *196*, 889–901. [CrossRef]

38. Ameri, M.; Jorjani, M. Performance assessment and multi-objective optimization of an integrated organic Rankine cycle and multi-effect desalination system. *Desalination* **2016**, *392*, 34–45. [CrossRef]
39. Druetta, P.; Aguirre, P.; Mussati, S. Minimizing the total cost of multi effect evaporation systems for seawater desalination. *Desalination* **2014**, *344*, 431–445. [CrossRef]
40. El-Dessouky, H.T.; Ettouney, H.M. *Fundamentals of Salt Water Desalination*; Elsevier: Amsterdam, The Netherlands, 2002; ISBN 9780444508102.
41. El-Dessouky, H.; Alatiqi, I.; Bingulac, S.; Ettouney, H. Steady-state analysis of the multiple effect evaporation desalination process. *Chem. Eng. Technol.* **1998**, *21*, 437–451. [CrossRef]
42. Pietrasanta, A.M.; Mussati, S.F.; Aguirre, P.A.; Morosuk, T.; Mussati, M.C. Optimization of a multi-generation power, desalination, refrigeration and heating system. *Energy* **2022**, *238*, 121737. [CrossRef]
43. Roosen, P.; Uhlenbruck, S.; Lucas, K. Pareto optimization of a combined cycle power system as a decision support tool for trading off investment vs. operating costs. *Int. J. Therm. Sci.* **2003**, *42*, 553–560. [CrossRef]
44. Marmolejo, J.A.; Velasco, J.; Selley, H.J. An adaptive random search for short term generation scheduling with network constraints. *PLoS ONE* **2017**, *12*, e0172459. [CrossRef]
45. UAE Ministry of Energy. UAE State of Energy Report. 2015. Available online: https://u.ae/en/information-and-services/environment-and-energy/water-and-energy/electricity (accessed on 1 March 2024).
46. SCAD. Energy and Water Statistics 2017. 2017. Available online: https://www.google.com/url?sa=t&source=web&rct=j&opi=89978449&url=https://www.scad.gov.ae/Release%2520Documents/Energy%2520and%2520Water%25202017%2520EN.pdf%20&ved=2ahUKEwiF6vOcjNiFAxVHlFYBHQk6A0oQFnoECBMQAQ&usg=AOv-Vaw1gEgkAs04DkYicMdp_HeGv (accessed on 1 April 2024).